# Hydrogen Bond in Layered Materials: Structural and Vibrational Properties of Kaolinite by a Periodic B3LYP Approach

Sergio Tosoni,[†] Klaus Doll,[‡] and Piero Ugliengo*[,†]

*Dipartimento di Chimica IFM, Università di Torino and NIS - Nanostructured Interfaces and Surfaces - Centre of Excellence, Via P. Giuria 7, 10125 Torino, Italy, and Institut für Mathematische Physik, TU Braunschweig Mendelssohnstraβe 3, D-38106 Braunschweig, Germany*

*Received January 28, 2006*

Extensive modeling of structural and vibrational properties of OH groups in kaolinite, a representative member of the clay family, has been studied within a periodic approach using the CRYSTAL03 program and adopting B3LYP functional with a polarized double-ζ Gaussian basis set. Optimized geometry and corresponding frequencies inclusive of the anharmonicity of all possible OH groups of kaolinite (inner, inner surface, and outer surface) are in overall good agreement with the structural and vibrational experimental data. Calculations definitely show that all inner surface OH groups are involved in weak interlayer hydrogen bonds, resulting in a B3LYP interlayer cohesive energy of about 32 kJ/mol per unit cell computed with a basis set of polarized triple-ζ quality. While the maximum error of the B3LYP OH stretching frequencies compared to experiment is around 20 $cm^{-1}$, exploration of the potential energy surface of the OH groups reveals that the large amplitude motion of some of them is possible at room temperature, which accounts for the presence of some broadness and extra bands in the infrared experimental OH stretching region. Calculations on a single kaolinite slab extracted from the bulk structure gives clear insight on the electrostatic complementary which holds the structure in place and allows the role of the OH groups at the external surface of layered materials to be understood.

## Introduction

Clay minerals are layered aluminosilicates, quite abundant in soils and sedimentary rocks. Every layer is composed of $TO_4$ tetrahedra (T = $Si^{4+}$, $Al^{3+}$, etc.) and $MO_6$ octahedra (M = $Al^{3+}$, $Fe^{3+}$, etc.). Different families are distinguished according to the tetrahedra/octahedra ratio; in 1:1 clay minerals, layers are held together via hydrogen bonds between hydroxyl groups attached to $MO_6$ groups and siloxane bridges belonging to $SiO_4$ tetrahedra, respectively.

The abundance of clay minerals in soils makes them relevant for environmental processes such as pollutant accumulation. In this respect, OH groups on layer surfaces (in virtue of their H-bonding ability) may play a decisive role in adsorption, intercalation, and catalysis phenomena.

A further extremely fascinating point is the role of clay minerals in prebiotic chemistry, which is a matter of long debate.[1−11] On one hand, various defects on aluminosilicates surfaces could have catalyzed peptide formation starting from single amino acids.[6,12] On the other hand, intercalation phenomena[3,4] could have protected the freshly formed peptides from hydrolysis, otherwise easily occurring in an aqueous environment.

In all these complex processes hydroxyl groups attached to the clay surfaces play an important role, on one hand by mediating interlayer interactions and, on the other hand, by hydrogen bonds with the adsorbed molecules at the outside surfaces. In that respect, the knowledge of their position in the structure is crucial. However, while heavy atom positions are accurately determined by X-ray experiments, that of the hydrogen atoms remain difficult to determine, as a result of their low atomic scattering factor. Quantum mechanical simulation can contribute to improving the experiments by providing a reliable portrait of OH groups and hydrogen bonds in clay minerals, as it has been done in the present work using an ab initio periodic approach, as implemented in the CRYSTAL code.[13]

Within the clays family, kaolinite is particularly attractive for simulation, because its relatively simple structure and small unit cell provide low computational cost, while all the interesting features of the surface OH groups forming interlayer hydrogen bonds are present. In particular, because Fourier transform infrared (FTIR) and Raman spectroscopy

[†] Università di Torino and NIS (http://www.nis.unito.it).
[‡] TU Braunschweig Mendelssohnstraβe 3.

(1) Rao, M.; Odom, D. G.; Orò, J. *J. Mol. Evol.* **1980**, *15*, 317.
(2) Lahav, N. *Heterog. Chem. Rev.* **1994**, *1* (2), 159.
(3) Smith, J. *Proc. Natl. Acad. Sci. U.S.A.* **1998**, *95*, 3370.
(4) Smith, J. *Proc. Natl. Acad. Sci. U.S.A.* **1999**, *96*, 3479.
(5) Boehme, C.; Marx, D. *J. Am. Chem. Soc.* **2003**, *125*, 13362.
(6) Aquino, A.; Tunega, D.; Gerzabek, M. H.; Lischka, H. *J. Phys. Chem. B* **2004**, *108*, 10120.
(7) Meng, M.; Stievano, L.; Lambert, J. F. *Langmuir* **2004**, *20*, 914.
(8) Basiuk, V. A.; Gromovoy, T. Y.; Golovaty, V. G.; Glukhoy, A. M. *Origins Life Evol. Biosphere* **1991**, *20*, 483.
(9) Basiuk, V. A.; Sainz-Rojas, J. *Adv. Space Res.* **2001**, *27*, 225.
(10) Basiuk, V. A. In *Encyclopedia of surface and colloid science*; Hubbard, A., Ed.; Marcel Dekker: New York, 2002; p 277.
(11) Ferris, J. P.; Hill, A. R., Jr.; Liu, R.; Orgel, L. E. *Nature* **1996**, *381*, 59.
(12) Rimola, A.; Tosoni, S.; Sodupe, M.; Ugliengo, P. *Chem. Phys. Lett.* **2005**, *408*, 295.
(13) Saunders, V. R.; Dovesi, R.; Roetti, C.; Orlando, R.; Zicovich-Wilson, C. M.; Harrison, N. M.; Doll, K.; Civalleri, B.; Bush, I. J.; D′Arco, P.; Llunell, M. *CRYSTAL03 User's Manual*; Università di Torino: Torino, 2003.

10.1021/cm060227e CCC: $33.50 
Published on Web 03/08/2006

are widely used to characterize hydrogen bonds in solids, this work is specifically devoted to the simulation of vibrational properties of OH groups in kaolinite. The background of the present discussion is based on many recently published papers on kaolinite, concerning synchrotron experiments,[14] vibrational spectroscopy studies,[15−19] and ab initio simulations.[20−25]

## Computational Methods

All calculations published in the present paper have been done using a development version of the CRYSTAL periodic code.[13] While the most common periodic codes use a plane waves basis set, CRYSTAL uses a local Gaussian basis set, allowing molecule, one-dimensional periodic polymers, two-dimensional periodic surfaces (slabs), and three-dimensional crystals (bulks) to be treated with the same level of theory. Commonly used density functional theory (DFT) methods, as well as Hartree−Fock and hybrid methods such as B3LYP, are implemented in CRYSTAL.

Previous works from our group[26,27] have shown that the choice of the Hamiltonian is critical when dealing with OH group vibrational properties, especially when they are involved in hydrogen bonds. B3LYP[28,29] has been shown to be definitely more reliable than other DFT methods, including the very popular PW91,[30−33] so it was adopted as the method of choice in the present work.

The basis set we have used is available on http://www.crystal.unito.it. Here, we report the exponents of the outer sp and d shells in bohr$^{-2}$: (1) Al, 85-11G* [34] ($\alpha_{sp}$ = 0.28; $\alpha_d$ = 0.47); (2) H, modified 3-1G* ($\alpha_s$ = 0.16; $\alpha_p$ = 1.1); (3) Si, 66-21G* [35] ($\alpha_{sp}$ = 0.13; $\alpha_d$ = 0.5); and (4) O, 6-31 G* with modified exponents ($\alpha_{sp}$ = 0.2742; $\alpha_d$= 0.6).

The Hamiltonian matrix is diagonilized in 8 *k* points, corresponding to a shrinking factor = 6.[36] Values (6, 6, 6, 6, 14) of the tolerances controlling Coulomb and exchange series have been adopted for all calculations. For accuracy check purposes, single point energy calculations have also been carried out with larger Coulomb/exchange tolerances (8, 8, 8, 8, 16) and with a larger basis set (hereafter referred as TZP) for the oxygen and silicon atoms (O, 8-411G*, $\alpha_{sp}$ = 0.181, $\alpha_d$ = 0.6; Si, 88-31G*, $\alpha_{sp}$ = 0.193, $\alpha_d$ = 0.61) designed by Nada and co-workers[37] and proved to give a small basis set superposition error (BSSE) and a 5-11G* for hydrogen ($\alpha_s$ = 0.14, $\alpha_p$ = 0.3) from Dovesi et al.,[38] whereas for Al an 88-311G* ($\alpha_{sp}$ = 0.14, $\alpha_d$ = 0.3) has been adopted.[39]

The exchange and correlation functional is integrated numerically on a grid of points. Integration over radial and angular coordinates is performed through Gauss−Legendre and Lebedev schemes, respectively. A pruned grid consisting of 75 radial points and 5 sub-intervals with (86, 194, 350, 974, 350) angular points has been used for all calculations (see option XLGRID in the CRYSTAL manual).[13] This grid corresponds to more than 410 000 integration points per unit cell and reduces the error to $8 \times 10^{-5}$ electrons per unit cell in the total integrated electron density (130 electrons).

The self consistent field (SCF) process has been stopped when the energy difference between cycles was smaller than $10^{-8}$ and $10^{-11}$ hartree in geometry optimizations and frequency calculations, respectively.

Internal coordinate optimization has been performed by using the Berny algorithm as it is implemented in CRYSTAL,[40,41] following a modified conjugated gradient algorithm formerly proposed by Schlegel.[42] Convergence is tested on the root-mean-square (RMS) and on the absolute value of the largest components of both the gradient and the estimated nuclear displacement. The threshold for the maximum and the RMS forces and the maximum and the RMS atomic displacements on all the atoms have been set to (in au) 0.000 45, 0.000 30, 0.001 80, and 0.001 20, respectively. The energy gradients relative to the cell parameters are then evaluated numerically,[43] and the whole process is reiterated until the above convergence criteria are satisfied.

In a periodic system and within the harmonic approximation the phonon frequencies at the Γ point are computed by diagonalizing the central zone ($k = 0$) mass weighted Hessian matrix:

$$W_{ij}(k=0) = \sum_G \frac{H_{ij}^{0G}}{\sqrt{M_i M_j}}$$


(14) Neder, R. B.; Burghammer, M.; Grasl, T.; Schulz, H.; Bram, A.; Fiedler, S. *Clays Clay Miner.* **1999**, *47*, 487.
(15) Johansson, U.; Frost, R. L.; Forsling, W.; Kloprogge, J. T. *Appl. Spectrosc.* **1998**, *52*, 1277.
(16) Frost, R. L.; Fredericks, P. M.; Kloprogge, J. T.; Hope, G. A. *J. Raman Spectrosc.* **2001**, *32*, 657.
(17) Frost, R. L.; Forsling, W.; Holmgren, A.; Kloprogge, J. T.; Kristof, J. *J. Raman Spectrosc.* **1998**, *29*, 1065.
(18) Johnston, C. T.; Sposito, G.; Birge, R. R. *Clays Clay Miner.* **1985**, *33*, 483.
(19) Franco, F.; Pérez-Maqueda, L. A.; Pérez-Rodrìguez, J. L. *J. Colloid Interface Sci.* **2004**, *274*, 107.
(20) Benco, L.; Tunega, D.; Hafner, J.; Lischka, H. *Chem. Phys. Lett.* **2001**, *333*, 479.
(21) Benco, L.; Tunega, D.; Hafner, J.; Lischka, H. *J. Phys. Chem. B* **2001**, *105*, 10812.
(22) Benco, L.; Tunega, D.; Hafner, J.; Lischka, H. *Am. Mineral.* **2001**, *86*, 1057.
(23) Hess, A. C.; Saunders, V. *J. Phys. Chem.* **1992**, *96*, 4367.
(24) Balan, E.; Saitta, A. M.; Mauri, F.; Calas, G. *Am. Mineral.* **2001**, *86*, 1321.
(25) Balan, E.; Lazzeri, M.; Saitta, A. M.; Allard, T.; Fuchs, Y.; Mauri, F. *Am. Mineral.* **2005**, *90*, 50.
(26) Pascale, F.; Tosoni, S.; Zicovich-Wilson, C. M.; Ugliengo, P.; Orlando, R.; Dovesi, R. *Chem. Phys. Lett.* **2004**, *396*, 308.
(27) Ugliengo, P.; Pascale, F.; Merawa, M.; Labeguerie, P.; Tosoni, S.; Dovesi, R. *J. Phys. Chem. B* **2004**, *108*, 13632.
(28) Becke, A. D. *J. Chem. Phys.* **1993**, *98*, 5648.
(29) Lee, C.; Yang, W.; Parr, R. G. *Phys. Rev. B* **1988**, *37*, 785.
(30) Perdew, J. P.; Wang, Y. *Phys. Rev. B* **1986**, *33*, 8800.
(31) Perdew, J. P.; Wang, Y. *Phys. Rev. B* **1989**, *40*, 3399.
(32) Perdew, J. P. *Electronic Structure of Solids*; Akademie Verlag: Berlin, 1991.
(33) Perdew, J. P.; Wang, Y. *Phys. Rev. B* **1992**, *45*, 13244.
(34) Catti, M.; Valerio, G.; Dovesi, R.; Causà, M. *Phys. Rev. B* **1994**, *49*, 14179.
(35) Nada, R.; Catlow, C.; Dovesi, R.; Saunders, V. *Proc. R. Soc. London, Ser. A* **1992**, *436*, 499.
(36) Saunders, V.; Dovesi, R.; Roetti, C.; Orlando, R.; Zicovich-Wilson, C. M.; Harrison, N. M.; Doll, K.; Civalleri, B.; Bush, I. J.; D′Arco, P.; Llunell, M. *CRYSTAL03 (Development version)*; University of Torino: Torino, 2004.
(37) Nada, R.; Nicholas, J. B.; McCarthy, M. I.; Hess, A. C. *Int. J. Quantum Chem.* **1996**, *60*, 809.
(38) Dovesi, R.; Ermondi, C.; Ferrero, E.; Pisani, C.; Roetti, C. *Phys. Rev. B* **1984**, *29*, 3591.
(39) Harrison, N. M. Unpublished results.

where $H_{ij}^{0G}$ is the second derivative of the electronic + nuclear repulsion energy $E$ evaluated at equilibrium $u = 0$ with respect to the displacement $u_i = x_i - x_i^{\ddagger}$ of atom $A$ in cell 0 and displacement $u_j = x_j - x_j^{\ddagger}$ of atom $B$ in cell $G$ from their equilibrium positions $x_i^{\ddagger}$, $x_j^{\ddagger}$:

$$\sum_G H_{ij}^{0G} = \sum_G \left[\frac{\partial^2 E}{\partial u_i^0 \partial u_j^G}\right]_0 \quad i = 1, ..., 3N; \quad j = 1, ..., 3N$$

It must be noted that, once the Hessian matrix **H** is calculated, frequency shifts due to isotopic substitutions can be calculated without any extra computational cost by simply changing the $M_i$ and $M_j$ masses in the equation above. In the present case, deuterium substitutes for the protons of the hydroxyl groups.

The Hessian at $u = 0$ is computed by the analytical evaluation of the energy first derivatives $\Phi_j$ of $E$ with respect to the atomic displacements

$$\Phi_j = \sum_G v_j^G = \sum_G \frac{\partial E}{\partial u_j^G} \quad j = 1, ..., 3N$$

and by the numerical evaluation of $[\partial\Phi_j/\partial u_i^0]_0$ using the central-difference formula

$$\left[\frac{\partial \Phi_j}{\partial u_i^0}\right]_0 \approx \frac{\Phi_j(0, ..., u_i^0, ..., 0) - \Phi_j(0, ..., -u_i^0, ..., 0)}{2u_i^0}$$
$$i = 1, ..., 3N; \quad j = 1, ..., 3N$$

In this paper a step $u_i = 0.001$ Å has been adopted. More details on this topic can be found in ref [44]. In the present case all the optimized structures have been characterized by full calculation of the harmonic frequencies and classified either as minima (all positive Hessian eigenvalues) or as saddle points (one negative Hessian eigenvalue).

The procedure adopted in this work to compute the anharmonicity of the OH stretching modes has already been tested and discussed in previous papers[26,45−47]. It consists of the following steps: (i) The OH distance is treated as a pure normal coordinate decoupled with respect to all other modes. (ii) The total energy of the system is calculated for a set of OH values around equilibrium (−0.2/+0.3 Å), and a sixth order polynomial fit is used to interpolate these points. (iii) The one-dimensional nuclear Schrödinger equation is solved following the algorithm proposed by Lindberg[48] and coded in the program ANHARM[49] that produces the three lowest eigenvalues $E_0$, $E_1$, and $E_2$ that are then used to compute $\omega_{01} = E_1 - E_0$, $\omega_{02} = E_2 - E_0$, and $\omega_e x_e = (2\omega_{01} - \omega_{02})/2$. The above procedure has now been implemented in the CRYSTAL03 code and can be activated via the EXTANHA keyword.

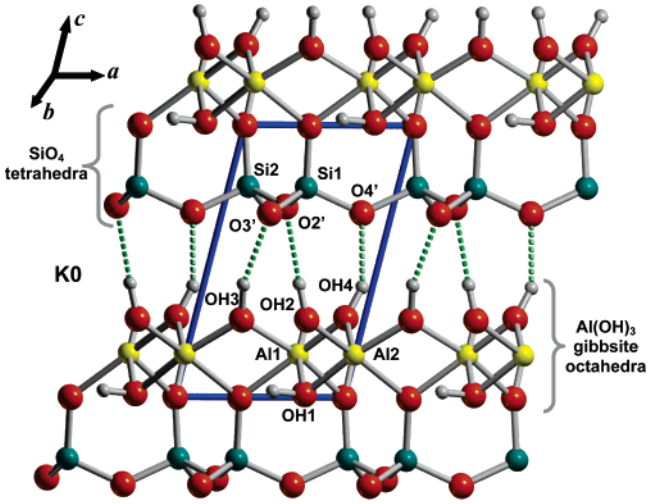


**Figure 1.** B3LYP optimized kaolinite bulk structure (K0) viewed along the crystallographic *b* axis. OH1 (inner group), OH2, OH3, and OH4 (inner surface groups). Hydrogen bonds as dotted lines.

## Structures and Energetics

Kaolinite is a layered aluminosilicate with a 1:1 Si/Al ratio and 17 atoms in its triclinic unit cell ($Al_2O_9Si_2H_4$) which crystallizes in the *C*1 space group. The layers stack along the *c* axis, and every layer is composed of a $SiO_4$ tetrahedra sheet connected to a gibbsite-like $Al(OH)_3$ one. Some of the OH groups belonging to the gibbsite sheet are hydrogen bonded to the siloxane bonds of the next layer (see Figure 1).

From inspection of Figure 1, two kinds of OH groups can be recognized: *inner* OH groups (OH1, buried in the layer) and *inner surface* OH groups (OH2, OH3, and OH4, connecting adjacent layers). A further case is that of the *outer surface* OH groups, which terminate the exterior crystal faces of any real crystal. All three kinds have been modeled here, inner and inner surface hydroxyls being present in the B3LYP optimized K0 bulk structure (see Figure 1). Outer hydroxyls are simulated enforcing periodic boundary conditions along *a* and *b* crystal directions only, defining an isolated single kaolinite layer slab extracted from the bulk K0 structure.

Cell parameters and internal degrees of freedom have been optimized for both the bulk and the isolated slab cases.

The experimental kaolinite structure, refined by Neder et al.,[14] has been taken from the ICSD database[50] (structure number 87771) and used as an initial guess for the geometry optimization, the resulting B3LYP bulk K0 structure being shown in Figure 1. The labeling of the OH groups is taken from a previous computational work on kaolinite from Benco

(40) Doll, K. *Comput. Phys. Commun.* **2001**, *137*, 74.
(41) Doll, K.; Harrison, N. M.; Saunders, V. *Int. J. Quantum Chem.* **2000**, *82*, 1.
(42) Schlegel, H. B. *J. Comput. Chem.* **1982**, *3*, 214.
(43) Zicovich-Wilson, C. M.; Pascale, F.; Catti, M. *LoptCGBerny (A Perl script for crystal structure optimization using CRYSTAL03)*; 2004, unpublished.
(44) Pascale, F.; Zicovich-Wilson, C. M.; Lopez, F.; Civalleri, B.; Orlando, R.; Dovesi, R. *J. Comput. Chem.* **2004**, *25*, 888.
(45) Merawa, M.; Civalleri, B.; Ugliengo, P.; Noel, Y.; Lichanot, A. *J. Chem. Phys.* **2003**, *119*, 1045.
(46) Merawa, M.; Labeguerie, P.; Ugliengo, P.; Doll, K.; Dovesi, R. *Chem. Phys. Lett.* **2004**, *387*, 453.
(47) Tosoni, S.; Pascale, F.; Ugliengo, P.; Orlando, R.; Saunders, V.; Dovesi, R. *Mol. Phys.* **2005**, *103*, 2549.
(48) Lindberg, B. *J. Chem. Phys.* **1988**, *88*, 3805.
(49) Ugliengo, P. *ANHARM-A program to solve monodimensional nuclear Schroedinger equation*; 1989, unpublished.
(50) Fachinformationzentrum (FIZ) Karlsruhe. Inorganic Crystal Structure Database (http://icsdweb.fiz-karlsruhe.de/), accessed Nov 2005.

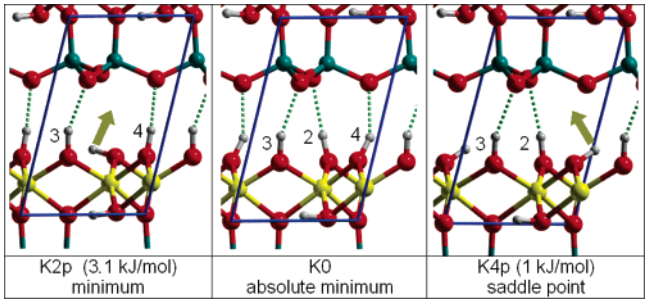


**Figure 2.** B3LYP K2p (minimum, 3.1 kJ/mol above K0), K0 absolute minimum, and K4p (saddle point, 1.0 kJ/mol above K0) optimized structures. The arrows show the proton involved in the definition of each structure.

et al.[21] All inner surface hydroxyls are involved in the hydrogen bond, in agreement with the experiment, while the calculation by Benco et al.[21] only gives two interlayer hydrogen bonds (involving OH3 and OH4), the OH2 being parallel to the layer. In the same work, proton dynamics simulations at 300 K showed that OH2 continuously rotates between vertical and horizontal positions. Experimentally, the increase of spectral resolution in the OH stretching region while decreasing the temperature seems to support this theory. However, in ref 22 no information was provided about the energy barrier between these two positions.

The CRYSTAL code does not allow molecular dynamics to be performed so that only the static exploration of the potential energy surface (PES) is possible. The outcome of PES exploration is reported in Figure 2, in which two new structures (K2p and K4p) have been characterized as PES stationary points. When compared to the full minimum one (K0, Figure 1) they are 3.1 and 1.0 kJ/mol higher in energy, respectively. Further vibrational analysis (vide infra) has shown that while both K0 and K2p structures are true minima, K4p is a saddle point. Both K2p and K4p are so close in energy to the full K0 minimum structure that all of them are expected to contribute at room temperature. All attempts to find different configurations failed in that all collapsed to one of the three already described. With CRYSTAL code it is still not possible to explicity search for saddle points during the energy optimization. However, considering that the transformation between K0 and K2p minima corresponds to rotation of the OH2 bond without any making/breaking of chemical bonds (see Figure 2), one should expect an energy barrier between K0 and K2p close to the energy difference (i.e., sligthly larger than 3 kJ/mol). Because the energy differences between K0, K2p, and K4p are so small, a check for the basis set dependence and the quantum treatment of the Coulomb/exchange series has been carried out. On one hand, single point energy calculations have been run on the optimized B3LYP/6-31G(d,p) geometries of K0, K2p, and K4p structures with the polarized TZP basis set described in the computational section (vide infra), and on the other hand, a single point energy calculation at B3LYP/6-31G(d,p) level has been run using the (8, 8, 8, 8, 16) tolerances for the Coulomb/exchange series. Results show, in all cases, that the order of stability (K0 < K4p < K2p) found at B3LYP/6-31G(d,p) is confirmed. Basis set improvement changes the instability of K4p and K2p with respect to K0 to 2.5 and 3.4 kJ/mol, respectively (to be compared with the smaller basis set values of 1.0 and 3.1 kJ/mol). Energy changes from the tolerance improvement are even smaller, resulting in 1.3 and 3.5 kJ/mol for K4p and K2p, respectively, sligthly higher than the values computed at B3LYP/6-31G(d,p) with standard tolerances. This shows that, even if the energy differences are small, the adopted method and basis set are robust enough to give physically sound results.

As already pointed out, the full frequency calculation characterizes the K4p structure as a saddle point (imaginary frequency: $-83$ cm$^{-1}$), and inspection of the associated eigenvector shows displacements entirely due to the H4 atom of the OH4 hydroxyl. Any small perturbation of the H4 position following the eigenvector direction toward the K0 minimum smoothly transforms K4p structure in the K0 minimum barrierless. On the other hand, any attempts to locate the second minimum for positions of the OH4 almost parallel to the gibbsite layer were unsuccessful. Our strategy was to set up the spatial steps taken by the optimizer to very small values and to start a new optimization by setting up the OH4 position to lie almost parallel to the gibbsite layer. During the full optimization, the OH4 group is brought back toward the position assumed in the K4p structure. However, total energy changes during the optimization were less than 0.1 kJ/mol! It is clear that the corrugation of the PES around the K4p is competing with the numerical accuracy of our calculation, in that large amplitude displacements are associated with almost no change in the total energy. This not only affects the precision in locating stationary points but also the calculation of the frequencies for very low wavenumbers. It is worth remembering that similar problems are also common in molecular calculations, when soft motion associated to some groups is present. In conclusion, we expect the minimum to be close to K4p based on the actual computational methodology. However, even if a minimum could be located in proximity to the K4p structure, it will not show any dramatically different feature (like the set of frequencies) compared to those already present in the K4p structure, because of the flatness of the PES.

Comparison between synchrotron experiment,[14] previous PW91 computational data,[22] and our data for the K0 configuration is shown in Table 1. The agreement between B3LYP optimized cell parameters and the experimental ones is very good. In that respect it is worth noting that even small distortions of the unit cell angles will cause large energy increments, showing that the PES relative to the cell shape is steep enough to ensure a well characterized minimum structure. The *c* value, which controls the interlayer distance and results from the weak H bonds and dispersive contributions, is slightly overestimated. This is no surprise, because purely dispersive contributions are missing in the definition of GGA functionals such as PBE, PW91, or BLYP, as well as by all hybrid functionals like the presently adopted B3LYP.[51,52]

Synchrotron measurements of OH distances[14] are critical, giving values that are too short in the range 0.75−0.88 Å. A more accurate comparison between calculations and

(51) Wu, X.; Vargas, M. C.; Nayak, S.; Lotrich, V.; Scoles, G. *J. Chem. Phys.* **2001**, *115*, 8748.
(52) Walsh, T. *Phys. Chem. Chem. Phys.* **2005**, *7*, 443.

**Table 1. Experimental and Calculated Geometrical Features of Kaolinite (Structure K0)[a]**

| | | B3LYP (this work) | | PW91[22] | |
|---|---|---|---|---|---|
| parameter | experiment[14] | bulk | slab | bulk[b,c] | slab[b] |
| *a* | 5.17 (5.15) | 5.19 (5.17) | 5.15 | | |
| *b* | 5.15 (8.94) | 5.17 (8.98) | 5.14 | | |
| *c* | 7.39 (7.39) | 7.43 (7.43) | | | |
| α | 84.2 (91.9) | 84.2 (91.9) | | | |
| *β* | 99.1 (105.0) | 99.1 (105.0) | | | |
| *γ* | 59.9 (89.8) | 59.9 (89.8) | 60.0 | | |
| OH1 | 0.75 | 0.969 | 0.963 | 0.991 | 0.987 |
| OH2 | 0.75(6) | 0.964 | 0.961 | 0.990 | 0.985 |
| OH3 | 0.77(9) | 0.965 | 0.961 | 0.987 | 0.985 |
| OH4 | 0.88(7) | 0.962 | 0.971 | 0.990 | 0.993 |
| O2···O2′ | 3.088(3) | 3.031 | | 2.910 | |
| O3···O3′ | 2.989(3) | 2.952 | | 3.050 | |
| O4···O4′ | 2.953(3) | 2.904 | | 2.843 | |
| OH2···O2′ | 173.3 | 165.9 | | 162.7 | |
| OH3···O3′ | 160.1 | 161.2 | | 162.7 | |
| OH4···O4′ | 141.8 | 152.7 | | 161.6 | |
| Al1−OH1 | 1.920 | 1.926 | 1.874 | | |
| Al1−OH2 | 1.849 | 1.862 | 1.916 | | |
| Al1−OH3 | 1.853 | 1.860 | 1.916 | | |
| Al1−OH4 | 1.862 | 1.856 | 1.914 | | |
| Al2−OH1 | 1.920 | 1.925 | 1.875 | | |
| Al2−OH2 | 1.854 | 1.864 | 1.915 | | |
| Al2−OH3 | 1.867 | 1.854 | 1.916 | | |
| Al2−OH4 | 1.854 | 1.854 | 1.914 | | |
| Si1−O1(octa) | 1.605 | 1.622 | 1.652 | | |
| Si1−O2′ | 1.622 | 1.641 | 1.625 | | |
| Si1−O3′ | 1.616 | 1.643 | 1.632 | | |
| Si1−O4′ | 1.615 | 1.646 | 1.631 | | |
| Si2−O2(octa) | 1.610 | 1.619 | 1.652 | | |
| Si2−O2′ | 1.619 | 1.640 | 1.631 | | |
| Si2−O3′ | 1.617 | 1.646 | 1.625 | | |
| Si2−O4′ | 1.628 | 1.642 | 1.632 | | |

[a] Bond lengths in angstroms, bond angles in degrees. Cell parameters refer both to the CRYSTAL primitive cell and, in parentheses, to the crystallographic cell. Labeling as in Figure 1. [b] Cell parameters fixed to the experimental ones. [c] Data refer to the "vertical" OH configuration. See ref 22 for details.

experiment derives from the distances between the oxygen atoms involved in the hydrogen bonds. In this case, a fair agreement between the present data and the experiment results exists: in particular, the B3LYP data, at variance with PW91 ones,[21] indicate that the shorter hydrogen bond is O4···O4′, the one involving the OH4 bond, followed by O3···O3′ and O2···O2′ (see Figure 1 and Table 1).

The comparison between B3LYP and PW91 data shows that the latter Hamiltonian overestimates the OH bond lengths and underestimates the O···O′ distances, as expected from previous experience on systems involving OH groups in hydrogen bond interaction.[27,53−55]

An important issue is the properties of the external surfaces of this material because they are responsible for the contact with molecular probes and may catalyze prebiotic chemical processes. Because the real material presents always both "internal" and true "external" surfaces, it is very hard to separate, in the experimental spectra, the features due to the "external" hydroxyl groups from those deriving from the

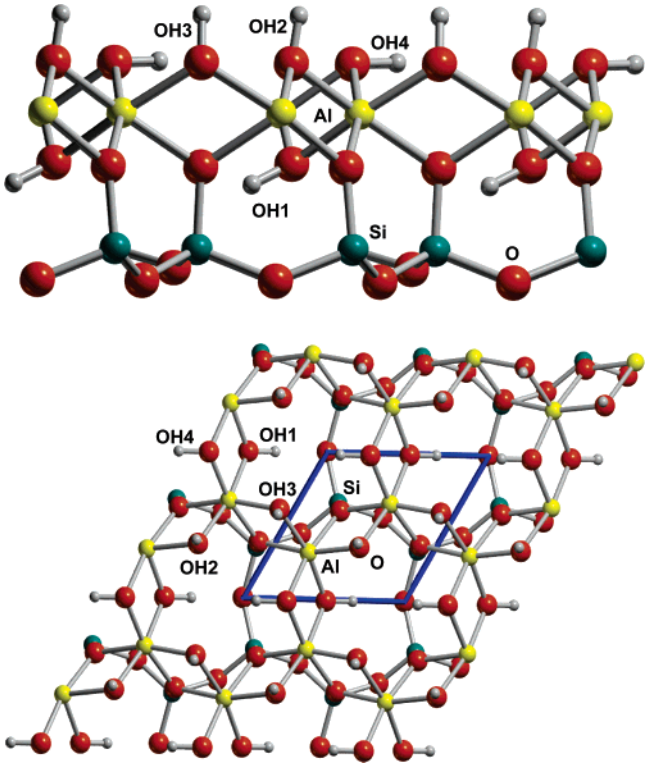


**Figure 3.** Lateral and top view of the B3LYP optimized kaolinite single isolated layer. OH1 (inner group), OH3, OH2, and OH4 (outer surface groups).

"internal" ones. Fortunately, simulation does not suffer from the above limit, being rather straigthforward to extract a single slab from the kaolinite bulk structure and compute the properties of such a "free" kaolinite surface (see Figure 3). The only assumption in this case is that the bulk underneath the real "external" surface, which is missing in the slab calculation, will not dramatically perturb the vibrational features of the "external" OH groups. It is worth noting that, at variance with the procedure adopted in the plane waves codes, our slab model does not include images above and below the reference slab and the system is a true bidimensional crystal.[56]

The comparison between the slab features computed here with the B3LYP functional and those obtained with the PW91 one by Benco et al.[21] reveals large similarities: in both cases one surface OH group (OH4) assumes an almost perfect horizontal position pointing to an opposite direction from OH1, whereas OH2 and OH3 remain in a vertical position (see Figure 3). Data in Table 1 also show the effect of the B3LYP full slab geometry relaxation: the Al−O bond distances show a significative elongation in the slab compared to the bulk values whereas the opposite is computed for the Si−O bond lengths. OH1, OH2, and OH3 all shorten slightly in the slab, whereas OH4 stretches. Explanation of some of these features will be accounted for in the next sections.

The calculation of the layer binding energy is defined as the energy needed to extract one layer from the kaolinite bulk, and its value is a function of the interlayer H-bond

(53) Mihaleva, V. V.; van Santen, R. A.; Jansen, A. P. J. *J. Phys. Chem. B* **2001**, *105*, 6874.
(54) O'Malley, P. J.; Farnworth, K. J. *J. Phys. Chem. B* **1998**, *102*, 4507.
(55) Civalleri, B.; Garrone, E.; Ugliengo, P. *J. Phys. Chem. B* **1998**, *102*, 2373.
(56) Dovesi, R.; Civalleri, B.; Orlando, R.; Roetti, C.; Saunders, V. R. *Rev. Comput. Chem.* **2005**, *21*, 1.

strength and of the less specific electrostatic interslab interactions. The B3LYP value is 61 kJ/mol per unit cell, which decreases to 39 kJ/mol per unit cell after correcting for the BSSE (BSSE = 22 kJ/mol). Because the BSSE is so large due to the relative poverty of the 6-31G(d,p) basis set when dealing with intermolecular interactions, the same calculation has been repeated with the TZP basis set described in the computational section (vide infra). The uncorrected binding energy value becomes 42 kJ/mol per unit cell, which reduces to 32 kJ/mol per unit cell after counterpoise correction (BSSE = 10 kJ/mol), showing that the counterpoise corrected binding energy changes only moderately as a function of the adopted basis set (from 39 to 32 kJ/mol for 6-31G(d,p) and TZP basis sets, respectively). By considering that three interlayer hydrogen bonds are present in each unit cell, it accounts for about 11 kJ/mol per hydrogen bond, showing a rather weak acidic nature of the Al−OH groups. The computed value of the interlayer binding energy is, however, large enough to justify intercalation processes which can only take place in kaolinite when rather strong molecular probes such as dimethyl sulfoxide[57] or acetamide[58] are adopted, as also shown in a recent computational work.[59] Indeed, it is well-known that among clays, kaolinite is less prone to intercalation when compared, for instance, with montmorillonite. The different behavior of 1:1 and 2:1 clay minerals when phenomena such as intercalation and swelling are concerned is an interesting and promising topic for future development of the present work.

## OH Vibrational Features

The OH stretching spectral region of kaolinite has been investigated by FTIR[19] and Raman microprobe techniques.[15] Influences of excitation wavelength,[16] temperature,[15,60] and degree of crystallinity of the sample have been found to be remarkable but not dramatic. Comparison with calculations is carried out considering data recorded on highly ordered crystalline samples at low temperature, when available, even if recent theoretical attempts to mimic the band shape as a function of crystallites shapes has also been addressed.[24,25]

FTIR experiments[19] at room temperature report four distinct bands in this region, located at 3620, 3651, 3668, and 3694 $cm^{-1}$, respectively (see Table 2). Microprobe Raman measurements[15] at 77 K also show four main bands (3615, 3656, 3675, and 3699 $cm^{-1}$, respectively, see Table 2), in reasonable agreement with the FTIR data. Measurements at room temperature performed in the same work showed that all bands are affected by temperature, with variations in frequencies between 5 and 10 $cm^{-1}$. The assignments suggested in refs 15 and 19 are the same: the band at 3620 $cm^{-1}$ is assigned to the stretching of the inner OH1 group. Assignment of the latter three bands has still not fully been achieved. The debate focuses on two interpretations: either in-phase/out-of-phase combinations of all the outer surface hydroxyls stretches or a series of decoupled OH2, OH3, and OH4 oscillators, giving rise to three separate bands. Some help in the assignment comes from selective deuteration studies,[61] which distinguish between inner and inner surface OH groups as a result of the different exchange kinetics: inner surface hydroxyls are more available for substitution and exchange their protons much faster than inner OH groups.

**Table 2. Experimental and Calculated OH Frequencies[a]**

| assignment | $\nu$(OH4) | $\nu$(OH2) | $\nu$(OH3) | $\nu$(OH1) |
|---|---|---|---|---|
| FTIR ($T$ = 298 K)[19] | 3694 | 3668 | 3651 | 3620 |
| Raman ($T$ = 77 K)[15] | 3699 | 3675 | 3656 | 3615 |
| $\omega_h$(K0) | 3895 | 3859 | 3842 | 3809 |
| $\omega_{01}$(K0) | 3714 | 3671 | 3657 | 3635 |
| $\omega_{01}$(K2p) | 3608 | 3708 | 3617 | 3678 |
| $\omega_{01}$(K4p) | 3791 | 3638 | 3623 | 3650 |
| $\omega_{01}$(slab) B3LYP | 3601 | 3751 | 3750 | 3717 |
| $\nu$(slab) PW91[21] | 3780 | 3954 | 3960 | 3856 |

[a] Harmonic ($\omega_h$) and fundamental ($\omega_{01}$) frequencies at B3LYP; PW91 data computed as a Fourier transform of the velocity autocorrelation function. All data in $cm^{-1}$.

Further insight on the assignment is provided by the present B3LYP calculation of the vibrational spectra of the considered structures. In that respect, the coupled/uncoupled nature of the four OH modes has been analyzed in two ways. First, by the potential energy distribution (PED) analysis of the involved vibrational modes, as provided by the CRYSTAL code. The PED analysis of the relevant modes of the full harmonic vibrational spectrum of the K0 structure revealed that the four highest frequencies are due to pure decoupled OH stretching modes (see Table 2, $\omega_h$ values). Second, isotopic substitution of the H by D atoms for the OH groups (leaving in turn one OH upon three OD group) gives OH harmonic frequencies which are 3808, 3858, 3846, and 3891 $cm^{-1}$ for OH1, OH2, OH3, and OH4, respectively, that is, pratically indistinguishable from the "fully coupled" values of the unsubstituted kaolinite (see Table 2, $\omega_h$ values). In conclusion, the above analysis of the harmonic frequencies has established that the four OH bands are due to uncoupled oscillators. This, in turn, allows for the calculation of the four fundamental $\omega_{01}$ bands, by using the fully decoupled anharmonic analysis as described in the computational section. Results shown in Table 2 revealed that the B3LYP values for the K0 structure are in fair agreement with experiment, the maximum deviation from the experiment being 20 $cm^{-1}$. As mentioned before, the experimental isotopic substitution of H by D allows only the band at 2672 $cm^{-1}$ to be assigned to the OH1 stretch whereas the inner surface hydroxyl stretching modes fall at 2695, 2708, and 2723 $cm^{-1}$. B3LYP results confirm the experimental assignment, giving values of 2683 $cm^{-1}$ for the OH1 mode, and also allow the stretching modes at 2702, 2713, and 2742 $cm^{-1}$ to be assigned to OH3, OH2, and OH4, respectively.

Careful inspection of the experimental Raman spectrum in refs 15 and 16 revealed that more than the four expected OH stretching bands are present. The presence and the number of the extra bands is also a function of the sample

(57) Frost, R. L.; Kristof, J.; Horvath, E.; Kloprogge, J. T. *J. Phys. Chem. A* **1999**, *103*, 9654.
(58) Frost, R. L.; Kristof, J.; Horvath, E.; Kloprogge, J. T. *Phys. Chem. Miner.* **1999**, *26*, 257.
(59) Michalkovà, A.; Tunega, D.; Turi-Nagi, L. *J. Mol. Struct. (THEOCHEM)* **2002**, *581*, 37.
(60) Frost, R. L.; Kloprogge, J. T. *J. Raman Spectrosc.* **2000**, *31*, 415.
(61) Johansson, U.; Holmgren, A.; Forsling, W.; Frost, R. L. *Analyst* **1998**, *123*, 641.

treatment so that their origin is unclear and still a matter of debate. Different suggestions have been made, spanning from transverse-longitudinal optical splitting to combinations of symmetric and antisymmetric motions. A possible origin of the band complexity and of the multiplicity in the number of OH bands may be rationalized by the coexistence of structures close in energy but with a different OH disposition. Good candidates are the K2p and the K4p structures already described above and displayed in Figure 2. K2p is a true minimum lying 3 kJ/mol above the K0 full minimum whereas K4p is a saddle point, only 1 kJ/mol above the full minimum. Both structures are expected to be present in moderate amounts at room temperature, contributing to the broadening of the vibrational spectrum. Table 2 collects the $\omega_{01}$(OH) frequencies for K2p and K4p showing values different enough from those of K0 to justify the final spectrum complexity.

From classical literature on the H bond,[62] it is expected that the shorter the intermolecular O···O′ distance and the closer to linearity the O−H···O′ angle, the higher the bathochromic shift suffered by the OH stretching frequency. Inspection of data in Table 1 reveals that while the O···O′ bond length follows the trend OH2 > OH3 > OH4 (from both experiments and calculations) the frequency shift (see Table 2) follows a different one, that is, OH4 > OH2 > OH3. This can be attributed to a rather distorted O−H···O′ angle (∼153°) for the OH4 case which causes a smaller bathochromic shift in comparison with those of OH2 and OH3, both sporting O−H···O′ angles closer to 180°.

A further element contributing to the complex nature of the observed vibrational spectra is that in the real material, some OH groups may belong to an "outer" surface, that is, to a surface which is no longer hydrogen bonded to the next layer. The B3LYP frequencies of the OH groups belonging to the "outer" surface are listed in Table 2, as computed for an isolated kaolinite slab whose geometry has been fully optimized. Direct comparison with experiment is not possible, but results are still interesting when compared with those computed for the bulk. Data obtained with the PW91 functional by Benco et al.[21] are also reported in Table 2, which have been computed as the Fourier transform of the velocity autocorrelation function. B3LYP results show that OH2 and OH3, which in the slab are both in a vertical position and obviously not interacting with the next layer (see Figure 3), have stretching modes suffering a strong hypsochromic shift compared to the bulk values (see Table 2), by 80 and 107 $cm^{-1}$, respectively. Also OH1 frequency undergoes a hypsochromic shift, passing from 3635 $cm^{-1}$ in the bulk to 3717 $cm^{-1}$ in the slab, as resulting from a different angle formed with the basal oxygen plane. This result is in agreement with the OH1 frequencies of different bulk structures (K2p and K4p), in which the frequency undergoes a hypsochromic shift proportional to the change of the angle defined by OH1 with the oxygen basal plane. On the contrary, OH4 shows a bathochromic shift from the value of 3714 $cm^{-1}$ in the bulk down to the value of 3601 $cm^{-1}$ in the slab. Comparing the K0 bulk structure (Figure 1) with that of the slab (Figure 3), it is evident that OH4 assumes a horizontal position in the slab, which enjoys stabilizing interactions with the surrounding basal oxygens, similar to what happens to OH1 in the K0 bulk structure. These interactions are affecting to a larger extent the OH frequencies than those due the weak hydrogen bond formed by OH4 with the single O4′ oxygen belonging to the next kaolinite layer.

## Electrostatic Potential Maps

It is well-known that the electrostatic potential at the surface of a solid material often plays an important role in determining the structure and energetics of adsorbates. Even for the very simple case of the (001) MgO surface, the key role of the surface electrostatic potential on the vibrational features of the adsorbed CO molecule has been well-established.[63,64]

In layered minerals, in which weak interactions are at the origin of the interlayer cohesion, it is interesting to study the complementary nature of the electrostatic potential between different layers. Furthermore, electrostatic potential maps can be of great help to understand adsorption processes occurring at the terminal faces of layered materials, a fact extremely relevant for the understanding of recent experiments in which DNA macromolecules have been adsorbed on layered materials.[65]

At first, the nature of the electrostatic potential in the K0 bulk structure in proximity to the basal $SiO_4$ plane and of the $Al(OH)_3$ (OH2, OH3, OH4) inner surface region has been studied. The calculation has been done by comparing the quantum mechanical electrostatic potential maps above and below a single kaolinite layer, rigidly extracted from the K0 bulk. Figure 4 shows the result: as expected, the $SiO_4$ basal plane and the inner $Al(OH)_3$ surface show, respectively, negative and positive regions of the electrostatic potential. By assuming that the electrostatic potential will not be dramatically altered once the slab is inserted into the bulk, the layered nature of the kaolinite along the *c* axis is derived quite naturally from the complementary nature of the two external faces of each slab.

Besides the maps, the average values of the electrostatic potential on two planes parallel to the slab and located above and below the slab (at large distances) have also been computed (keyword POTC/ICA = 2 of the CRYSTAL03 properties module) to quantify the dipolar character of each slab. The difference in the electrostatic potential computed on the two parallel and distant planes changes from 8 V, for the slab rigidly extracted from the bulk, to 3 V, for the isolated optimized slab, as a consequence of the geometry relaxation. In Figure 5, the electrostatic potential of the slab rigidly extracted from the K0 bulk structure (upper side) is contrasted with that resulting from a fully optimized slab (lower side). Clearly, geometry relaxation brings about a rather complex structural change, which affects both the

(62) Jeffrey, G. A. *An introduction to hydrogen bonding*; Oxford University Press: Oxford, 1997.
(63) Damin, A.; Dovesi, R.; Zecchina, A.; Ugliengo, P. *Surf. Sci.* **2001**, *479*, 255.
(64) Pacchioni, G. *Surf. Rev. Lett.* **2000**, *7*, 277.
(65) Valdrè, G.; Antognozzi, M.; Wotherspoon, A.; Miles, M. J. *Philos. Mag. Lett.* **2004**, *84*, 539.

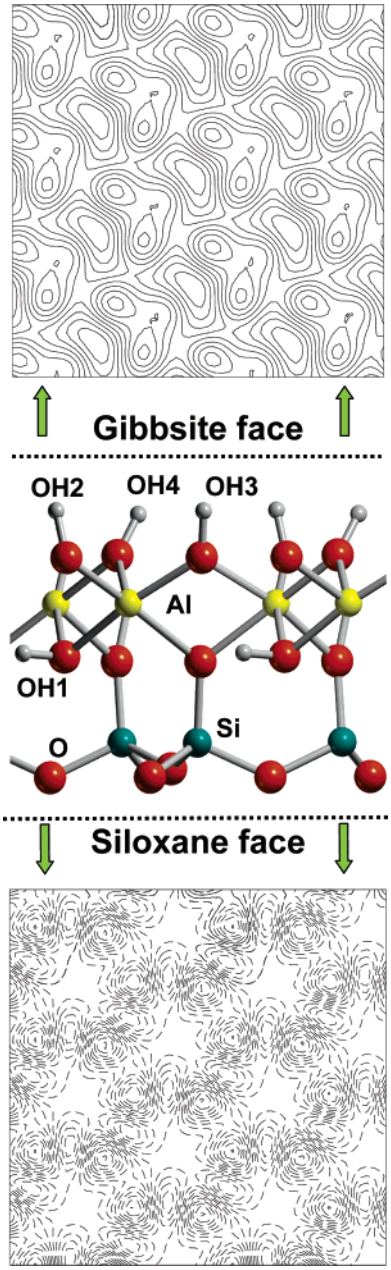


**Figure 4.** B3LYP electrostatic potential maps computed 2 Å above and below the surfaces of a single kaolinite layer. Isolines (continuous lines, positive values; dashed lines, negative values) drawn at each 0.001 au.

topology and the long-range value of the electrostatic potential, mainly due to the rotation of both OH4 and OH1 hydroxyls. The former moves, so that a weak hydrogen bond with the oxygen atom of the nearby OH4 group is established. This is also evidenced by the large bathochromic shift of the OH4 stretching frequency compared to the value in the K0 structure (from 3714 to 3601 $cm^{-1}$, vide infra, and also Table 2). As for the OH1 group, geometry relaxation moves it out of the plane defined by the six nearby oxygen atoms. Inspection of the B3LYP electrostatic potential (see Figure 6) computed for the rigidly extracted slab in the oxygen plane near the OH1 group reveals a rather favorable electrostatic interaction of the H1 proton with the negative basins due to the oxygen atoms, which is partly lost when the geometry of the slab is fully optimized. This, in turn, causes a large hypsochromic shift of the OH1 frequency in

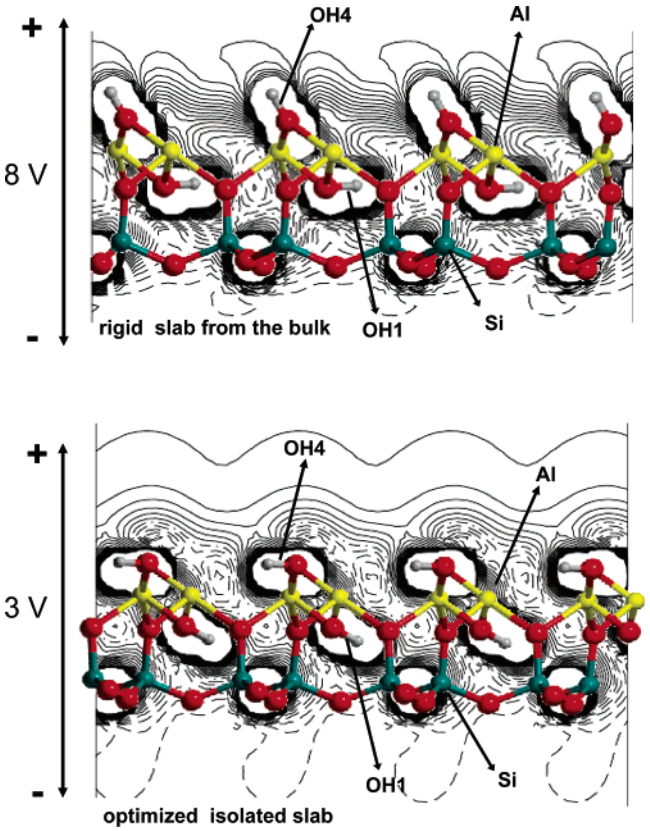


**Figure 5.** Comparison between B3LYP electrostatic potential maps computed in the OH1−OH4 plane for a slab rigidly extracted from the bulk and for an isolated and fully optimized one. Also shown are the values (in volts) of the difference in the averaged electrostatic potential computed on two distant planes parallel to the slab.

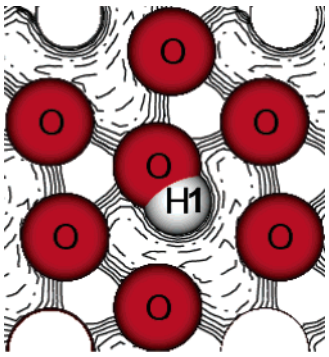


**Figure 6.** Electrostatic potential map in the basal oxygens plane of the K0 structure. The hexagonal arrangement of oxygen atoms surrounding every inner OH1 hydroxyl group shows a negative region of the electrostatic potential (dashed lines) in close proximity of the H1 atom. Isolines drawn at each 0.01 au.

the optimized slab when compared to the value computed for the K0 structure (from 3635 to 3717 $cm^{-1}$, see Table 2).

## Conclusions

In this work, structural and vibrational properties of OH groups in kaolinite have been studied ab initio using the B3LYP functional and polarized double-ζ quality Gaussian basis as encoded in the CRYSTAL03 program. Single point energy calculations with a polarized triple-ζ quality basis set TZP have also been carried out to validate the reliability of the order of stability of the considered structures, as computed at the B3LYP/6-31G(d,p) level. Good agreement

with synchrotron experiment has been obtained for the most stable structure (K0), both as far as cell parameters and internal coordinates are concerned. The K0 structure has all the inner surface OH groups H bonded to the next layer, whereas the inner OH group is buried within the slab itself. Two other stationary points have been found (K2p as the minimum and K4p the as saddle point), showing only two H bonds in the unit cell with the layer above: the very small energy difference which separates K4p and K2p from the true minimum K0 (2.5 and 3.4 kJ/mol, respectively, computed with the TZP basis set) suggests their presence in moderate amount at room temperature, while excluding a detectable population at liquid nitrogen temperature.

Analysis of the B3LYP frequencies has allowed for convincing interpretations of the rather complex experimental spectra. PED of the modes associated to the OH stretching frequencies together with isotopic H/D substitution clearly indicates that each OH group contributes almost entirely to a given infrared band, that is, coupling between the OH stretching modes is totally negligible. Quantum anharmonic calculation of the OH frequencies of the uncoupled OH oscillators is in very good agreement with the experiment carried out at liquid nitrogen temperature, the maximum error being around 20 $cm^{-1}$.

Calculation on a single kaolinite slab extracted from the bulk structure has allowed the interlayer binding energy to be calculated and the vibrational features of the OH groups belonging to a truly external kaolinite surface always present in the real material to be studied. The 39 kJ/mol per unit cell (32 kJ/mol with the TZP basis set) needed to extract a layer from the kaolinite bulk is in agreement with the character of kaolinite rather resistant to swelling and intercalation, in line with experimental evidence. In the isolated slab, the absence of H bonds with the next layer causes rearrangements of the OH groups and brings about a hypsochromic shift of the OH1, OH2, and OH3 frequencies, whereas OH4 suffers a bathochromic shift as a result of favorable electrostatic interaction with the basal oxygens plane.

B3LYP electrostatic potential maps of a single kaolinite slab reveal its dipolar nature along the crystallographic *c* axis which is at the origin of the layered arrangement along that direction in kaolinite, as a result of the electrostatic complementary character of the two external faces of each slab. The electrostatic potential outside an isolated kaolinite slab is very sensitive to the geometry relaxation, the latter reducing quite dramatically the dipolar character of the slab rigidly extracted from the bulk structure.

**Acknowledgment.** The staff of the Theoretical Chemistry Research Group of the Torino University is kindly acknowledged for providing the development versions of the CRYSTAL code. CINECA supercomputing center is also acknowledged for allowance of computer time. S.T. acknowledges Fondazione CRT-Progetto Lagrange for funding his Ph.D. within the multidisciplinary research project on complex systems.

CM060227E